

Graphene ribbons for tunable coupling with plasmonic subwavelength cavities

Gilles Rosolen* and Bjorn Maes

Micro- and Nanophotonic Materials Group, Faculty of Science, University of Mons, Bat. IV, Avenue Maistriau 19, B-7000 Mons, Belgium

*Corresponding author: gilles.rosolen@umons.ac.be

Received February 7, 2014; revised March 14, 2014; accepted March 18, 2014;
posted March 19, 2014 (Doc. ID 206083); published April 16, 2014

Since graphene supports low loss plasmonic guided modes in the infrared range, we theoretically investigate the coupling of these modes in patterned sheets with nanocavities. We calculate cavity modes and (potentially critical) coupling in filter-type circuits, with resonances observed as multiple minima in the reflection spectrum. The origin and properties of the cavity modes are fully modeled by coupled mode theory, exploring for various positions of the cavity with respect to the access waveguide. A useful resonance frequency shift is examined by modifying the graphene doping (e.g., via voltage tuning). The deep subwavelength cavity modes reach quality factors up to 42 for ribbons of 30 nm width around 5 μm wavelength. These resonances provide opportunities for ultracompact optoelectronic circuits. © 2014 Optical Society of America

OCIS codes: (250.5403) Plasmonics; (230.7370) Waveguides; (230.5750) Resonators; (250.3140) Integrated optoelectronic circuits.

<http://dx.doi.org/10.1364/JOSAB.31.001096>

1. INTRODUCTION

Graphene is a promising material for a wide range of nanotechnological applications [1–3]. If we focus on the optoelectronic applications, functional graphene circuits using plasmonic modes form an interesting developing field [4]. In this paper, we describe the coupling of graphene plasmons between a semi-infinite sheet and a nanoribbon, which gives deep reflection dips at certain resonant wavelengths. The useful phenomenon of critical coupling leading to zero reflection from these cavities can be engineered. Furthermore, by tuning the gate voltage on graphene the resonant wavelength is adjusted. The width of the ribbon (only 75 nm or smaller) and the confinement of the plasmon mode (<50 nm) lead to ultrasmall, tunable optoelectronic circuits.

Since its discovery graphene has spurred tremendous interest for its electronic, mechanical, and optical properties. This one atom thick material has been used in many optical applications: in the optical range as a transparent conductor [5,6], in the far-infrared and terahertz frequencies as a building block to realize tunable metamaterials [7], and in the near-infrared to design optical sensors [8,9] or graphene plasmonic devices [10].

Indeed, in the infrared range graphene supports plasmon-like modes which can be less lossy and more confined than their noble metal counterparts [11]. In the meantime, the promise of photonics integrated circuits is jeopardized by limiting problems with downscaling and integration [10]. Consequently, graphene circuits create great interest for their tiny size (one atom thick material and very small plasmon wavelength λ_p < 50 nm [11]) and their tunability via electrostatic gating [12].

In recent work, plasmons in graphene nanoribbons were studied in [13]. Bends and splitters were discussed in [14], and directional couplers were demonstrated in [15], with a

switching behavior in [16]. Additionally, it was shown that curved graphene sheets support plasmons with low radiation losses leading to flexible graphene circuits [17].

Here, we study the coupling of graphene plasmons on a semi-infinite sheet with a nanoribbon (functioning as cavity) separated by an air-gap, and we show and explain tunable minima in the reflection spectra. To the best of our knowledge, these cavities have not been studied extensively.

The simulations are performed with COMSOL, a commercial finite-element-based software package. Graphene is modeled as a thin layer of 0.5 nm thickness and its optical parameters are defined via the relative permittivity: $\varepsilon_{\parallel}(\omega, E_F) = 1 + i\sigma(\omega, E_F)/(\varepsilon_0\omega t)$, where t is the thickness of the graphene sheet, E_F the Fermi energy, ω the angular frequency, and $\sigma(\omega, E_F)$ the optical surface conductivity (S/m^2) computed by the Kubo–Greenwood formula [18,19]. The scattering lifetime of electrons in graphene is fixed to $\tau_g = 10^{-12}$ s. We operate in the range $\omega = 2$ to 3×10^{14} rad/s and $E_F = 0.2$ to 1 eV (Fermi energies up to $E_F = 1 - 2$ eV have been reported [20]). The doping level can be employed to tune graphene. Note that optical properties of graphene are anisotropic [21,22]. We employed $\varepsilon_{\perp} = -3.8 - 0.70i$ in the direction normal to the surface of graphene. Nevertheless, this parameter has negligible influence on the results.

The paper describes the numerical and theoretical modeling of a small graphene ribbon operating as a cavity in various geometries. In the first section, the cavity is placed at the end of an access sheet or waveguide. Tunable minima in the reflection spectra are observed (Section 2.B) and described by the coupled mode theory (Section 2.A). In the following section, the cavity is next to the access waveguide. A directional-coupler-based theory is developed in Section 3.A, with simulation results in Section 3.B.

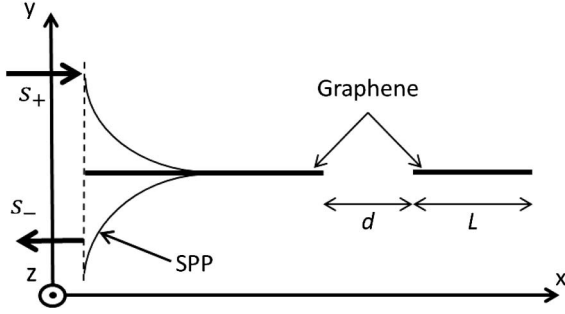


Fig. 1. Side view of the ribbon cavity.

2. RIBBON AT THE END OF A SHEET

In this section, we study a two-dimensional system composed of a semi-infinite sheet of graphene (the access waveguide) and a small ribbon (serving as the cavity) of width L at distance d from the sheet (Fig. 1). The background medium is air ($\epsilon_{\text{air}} = 1$).

Without the cavity, the injected plasmon propagates along the graphene sheet and is nearly totally reflected at the edge: the plasmon is so confined that very little light is radiated. When a cavity ribbon is placed near the end of the sheet, the evanescent field can couple into and light can resonate in the cavity [Fig. 2(a)]. For a specific wavelength, we observe a reflection minimum [Fig. 2(b)]. Note that the presented reflections are “normalized”: the losses in the access waveguide are neglected, but the losses in the cavity are accounted for.

A. Coupled Mode Theory

The properties of the cavity modes are modeled very adequately by the coupled mode theory (CMT). CMT describes the coupling of ports with resonators [23]. In our case, a single mode port couples with a cavity, with the coupling strength characterized by τ_c^{-1} . The dissipative and radiative losses occurring in the resonator are represented by τ_a^{-1} and τ_r^{-1} , respectively. The equations of temporal CMT are [23]

$$\frac{da}{dt} = \left(j\omega_0 - \frac{1}{\tau} \right) a + \sqrt{\frac{2}{\tau_c}} s_+, \quad (1)$$

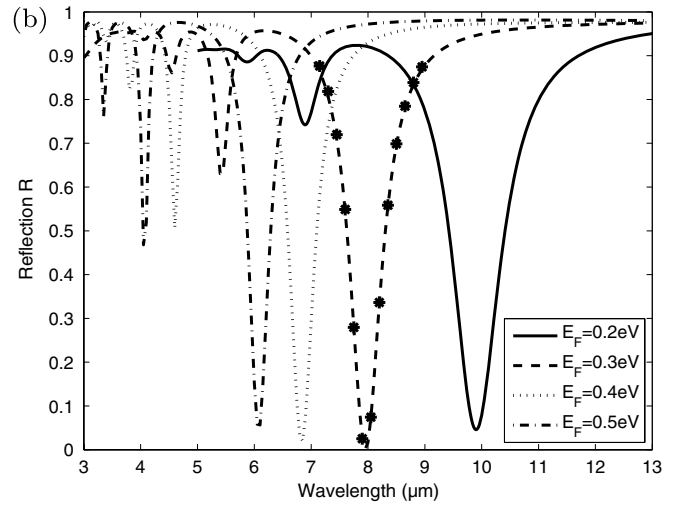
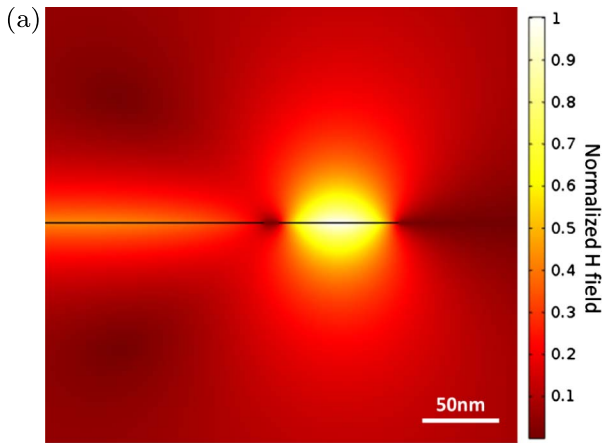
$$s_- = r_0 s_+ + \sqrt{\frac{2}{\tau_c}} a, \quad (2)$$

where s_+ and s_- are the input and output amplitudes of the (plasmon) mode transmitted through the port, a is the amplitude of the cavity mode, r_0 is the reflection at the edge of the graphene sheet without the resonator, and ω_0 is the resonant frequency. Note that $(1/\tau) = (1/\tau_c) + (1/\tau_a) + (1/\tau_r)$.

Isolating s_-/s_+ and going to the frequency domain ($e^{+j\omega t}$), we find

$$\frac{s_-}{s_+} = r_0 \left(1 - \frac{\frac{2}{\tau_c}}{j(\omega - \omega_0) + \frac{1}{\tau}} \right), \quad (3)$$

and finally



Doping (eV)	Fitted			Theoretical	
	τ_c (10^{-13} s)	τ_a (10^{-13} s)	ω_0 (10^{14} rad/s)	Q	τ_a (10^{-13} s)
0.2	2.6	1.7	1.9	9.2	1.7
0.3	2.0	2.0	2.4	12	2.0
0.4	1.7	2.2	2.8	13	2.3
0.5	1.5	2.3	3.1	13	2.4

Fig. 2. (a) Normalized $|H_z|$ field for $E_F = 0.3$ eV at $\lambda = 7.95$ μm . The size of the cavity is $L = 75$ nm and the distance from the sheet is $d = 10$ nm. (b) Simulated reflection spectrum for different doping (E_F). Theoretical points are shown for $E_F = 0.3$ eV. Three orders of resonances are shown for each E_F . (c) Table with fitted lifetimes and resonant frequency ω_0 , and the calculated absorption lifetime. The quality factors are computed from the fitted parameters as $Q = \omega_0/\Delta\omega_{\text{FWHM}}$.

$$R = \left| \frac{s_-}{s_+} \right|^2 = |r_0|^2 \frac{(\omega - \omega_0)^2 + \left(-\frac{1}{\tau_c} + \frac{1}{\tau_a}\right)^2}{(\omega - \omega_0)^2 + \left(\frac{1}{\tau_c} + \frac{1}{\tau_a}\right)^2}. \quad (4)$$

The Lorentzian-shaped resonance has its minimum at $\omega = \omega_0$. In addition, one obtains a useful critical coupling when $\tau_a = \tau_c$: all the energy coupled to the cavity is dissipated, and the reflection goes to zero.

As previously mentioned, because of the remarkable impedance mismatch between the plasmon and free space, radiative losses at the edge of a sheet can be neglected, so $|r_0|^2 \approx 1$ and $\tau_r^{-1} \approx 0$.

The absorption lifetime τ_a can be modeled via [24]

$$\tau_a = \frac{1}{v_g \Im(\beta)}, \quad (5)$$

where v_g is the group velocity of the considered mode and $\Im(\beta)$ is the imaginary part of its propagation constant.

B. Results and Discussion

In Fig. 2(b), the cavity has a size of $L = 75$ nm. The doping of graphene is shifted from $E_F = 0.2$ eV to $E_F = 0.5$ eV and we observe a shift of the fundamental resonance wavelength from $\lambda = 10$ to 6 μm . This could be realized by introducing a gate voltage on graphene (the sheet and the ribbon are doped in the simulations (doping only the cavity gives identical results, not shown here). Figure 2(c) shows different fitted parameters from the first-order minima of these spectra using Eq. (4), and the corresponding fit is shown in Fig. 2(b) for $E_F = 0.3$ eV (dots).

First of all, one observes that the theoretical absorption lifetime [Eq. (5)] matches the fitted value, which increases with the graphene doping. This is understood from the interband transitions in graphene, occurring above a threshold related to the Fermi energy ($\hbar\omega > 2E_F$) which can be shifted to higher frequencies by larger doping [12]. Subsequently increasing doping decreases interband transitions and thus decreases losses. This impacts the imaginary part of the graphene

plasmon propagation constant: doping graphene decreases its value and from Eq. (5) one finds an increase of τ_a .

Note that the absorption lifetime is correlated to the scattering lifetime τ_g of electrons in the graphene sheet. Theoretically [13], the latter can be determined by the equation $\tau_g = \mu E_F / ev_F^2 \approx E_F \times 10^{-12}$ s/eV, where the Fermi velocity $v_F \approx 10^6$ m/s and with the measured impurity-limited DC mobility $\mu \approx 1000$ cm²/(V s) [25]. For the sake of clarity, we arbitrarily fix $\tau_g = 10^{-12}$ s in the permittivity model but the minima are also observed for lower values of this parameter. This is illustrated in Fig. 3(a) for $E_F = 0.4$ eV (theoretically $\tau_g \approx 4 \times 10^{-13}$ s). Varying τ_g keeps the resonant frequency ($\omega_0 = 2.8 \times 10^{14}$ rad/s) and the coupling lifetime ($\tau_c = 1.7 \times 10^{-13}$ s) constant while τ_a changes. A limiting problem is that the minimum becomes wider with the losses.

Next, from Fig. 2(c) we note that τ_c decreases when increasing the doping level. This is explained by the confinement of the plasmon. As it will be demonstrated later, the resonances always occur for the same value of the real part of the propagation constant $\Re(\beta) = n_{\text{eff}}\omega/c$ (where c is the speed of light). This implies that n_{eff} decreases when omega increases, leading to a smaller confinement for larger angular frequencies. Since τ_c^{-1} theoretically stems from an overlap integral of the evanescent fields, this gives stronger coupling (τ_c smaller) when ω increases as shown in Fig. 2(c). Because of the integration model of τ_c^{-1} , the coupling lifetime is also tunable via the distance d , increasing with this parameter. This is shown in Fig. 3(b) for $E_F = 0.3$ eV, with all other parameters constant ($\omega_0 = 2.4 \times 10^{14}$ rad/s, $\tau_a = 2.0 \times 10^{-13}$ s).

Because of these evolutions of τ_a and τ_c , for the configuration of Fig. 2(b), critical coupling ($R = 0$) is reached when $\tau_a = \tau_c = 2.0 \times 10^{-13}$ s and $\omega = \omega_0 = 2.4 \times 10^{14}$ rad/s [see Eq. (4)]. Note that doping only the cavity will change the coupling and absorption lifetimes following the same trends as in Fig. 2(c). The equality $\tau_a = \tau_c$ will then be reached for another doping configuration. For instance, when the access waveguide is $E_F = 0.4$ eV doped and the cavity $E_F = 0.25$ eV, a critical coupling $R = 0$ is reached when $\omega_0 = 2.1 \times 10^{14}$ rad/s.

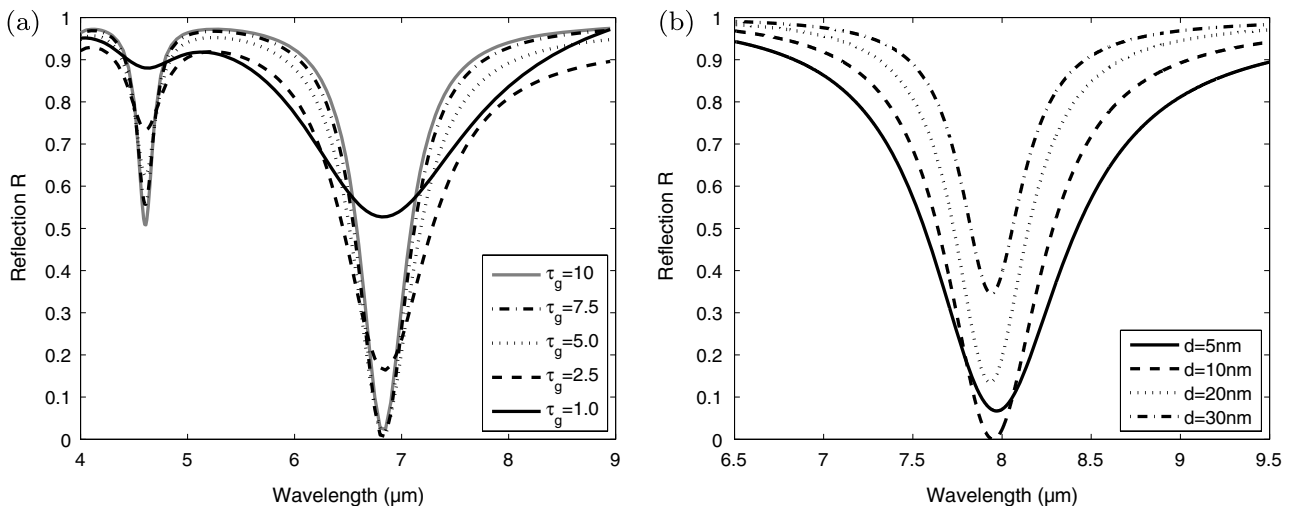


Fig. 3. Simulated reflection in function of the wavelength. (a) The resonances are modified with the scattering lifetime of the electrons in graphene. For the first-order minimum, critical coupling is obtained for $\tau_g = 7.5 \times 10^{-13}$ s (legend with τ_g in 10^{-13} s). $E_F = 0.4$ eV, $L = 75$ nm, and $d = 10$ nm. (b) The resonances depend on the cavity-waveguide distance d . A critical coupling is observed for $d = 30$ nm. $E_F = 0.3$ eV and $L = 75$ nm.

When examining the second-order minima [Fig. 3(a)] we do not reach critical coupling. Indeed, losses are too important at these wavelengths (τ_a too small in comparison to τ_c to reach $\tau_a = \tau_c$). Consequently, the minimum of reflection is only about 0.5. Note that for 0.4 eV doping, the second-order dip has a quality factor $Q = 15$. This value is higher than the one obtained for the first-order dip ($Q = 13$), but this is mainly due to the larger resonance frequency ω_0 .

The particular resonance frequency is strongly determined by the plasmon properties. Indeed, in order to get a resonance in the cavity one needs constructive interference during a round trip

$$2\Re\{\beta(\omega)\}L + 2\varphi_r = 2m\pi, \quad (6)$$

where β is the propagation constant of the plasmon mode, \Re indicates the real part, φ_r is the phase induced by the reflection at the end of the ribbon, and m is an integer. The first-order resonance is obtained when $m = 1$.

It turns out that φ_r is relatively constant (≈ 0.85 rad) in the typical mid-infrared range of frequencies, so for a particular L the resonance always occurs at the same value of the propagation constant $\Re\{\beta\} \approx 30$ rad/ μm . In Fig. 4, the graphene dispersion is plotted for different doping levels. The crossing between this value of $\Re\{\beta\}$ (vertical black line) with the different dispersion curves corresponds with the resonance frequencies fitted in the Fig. 2(c) from our simulations. This is a consequence of the specific properties of graphene: applying a gate voltage shifts the optical properties of the plasmon and thus the resonance frequency.

Thanks to these properties one can easily predict the resonance frequency for a given cavity length. For example, the gray straight vertical line (Fig. 4) at $\Re\{\beta\} = 76$ rad/ μm shows the expected resonances for a $L = 30$ nm length cavity, the first-order frequency for 1 eV doping will occur at $\omega_0 = 6.8 \times 10^{14}$ rad/s.

In order to improve the quality factor one would need smaller cavities, i.e., larger resonance frequencies. However, going in this direction increases the losses (interband transitions occur when $\hbar\omega > 2E_F$). To counter that effect a high doping of graphene is required, so when $E_F = 1$ eV a quality

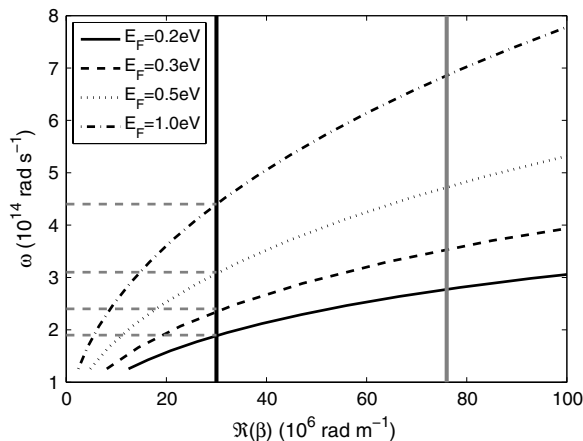


Fig. 4. Dispersion of the plasmon propagating along a graphene sheet for different doping levels. The black vertical line represents the required real part of β for a resonance in a 75 nm long cavity. The horizontal lines indicate the resonance frequencies. The vertical gray line stands for the expected resonances in a 30 nm cavity.

factor of $Q = 42$ is reached with a cavity of $L = 30$ nm, at $\lambda_0 = 2.8$ μm . This is the of the same order of magnitude of the quality factor of localized surface plasmon resonances of metals like silver ($Q \approx 30$) or gold ($Q \approx 10$) [26].

3. DIRECTIONAL COUPLER CAVITY

In this section, we study a graphene ribbon (cavity) on top of a free-standing semi-infinite graphene sheet (Fig. 5). Without the cavity the plasmon propagates along the semi-infinite graphene sheet, is reflected at the edge, and creates a stationary wave. If we put a ribbon on top of the sheet the plasmon can couple with this cavity, leading to more complex interference effects and resonances.

We introduce a simple model in the following subsection, and discuss the behavior and comparison with simulations in the next subsection.

A. Theory

The coupling between two parallel graphene sheets separated by a distance d can be described by directional coupler theory. We suppose that the two plasmonic waveguides are identically doped so that they support a plasmon with the same propagation constant β . The coupling between the plasmon modes is characterized by κ . The solution for the lossless case is in [27]. One can take the phase and the losses into account via the exponential factor $e^{-j\beta x}$

$$a_1(x) = [\cos(\kappa x)a_1(0) - j \sin(\kappa x)a_2(0)]e^{-j\beta x}, \quad (7)$$

$$a_2(x) = [-j \sin(\kappa x)a_1(0) + \cos(\kappa x)a_2(0)]e^{-j\beta x}, \quad (8)$$

where $a_i(x)$ are the amplitudes of the plasmonic mode in the i th waveguide, and x is the propagation direction.

In a first step, we propose a system with two ports. In Fig. 5, suppose that the reflection r_0 is handled by a port, with s_{2+} and s_{2-} the input and output amplitude of the mode transmitted through the port, respectively. With a cavity of length L separated a distance x_1 from port 1 and x_2 from port 2, the scattering matrix is

$$\begin{pmatrix} s_{1-} \\ s_{2-} \end{pmatrix} = \begin{pmatrix} S_1 & S_x \\ S_x & S_3 \end{pmatrix} \begin{pmatrix} s_{1+} \\ s_{2+} \end{pmatrix}, \quad (9)$$

where

$$S_i = \frac{-r_0 \sin^2(\kappa L)}{1 - (r_0 \cos(\kappa L) e^{-j\beta L})^2} e^{-2j\beta(L+x_i)}, \quad (10)$$

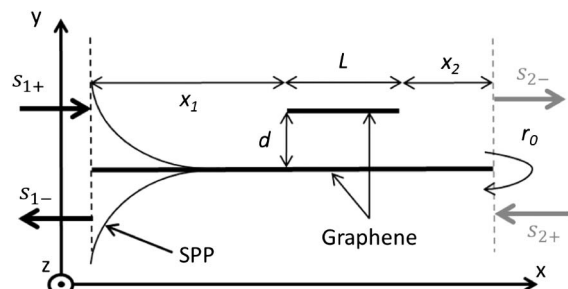


Fig. 5. Transversal view of the studied structure.

$$S_x = \cos(\kappa L) e^{-j\beta(x_1+L+x_2)} \frac{1 - r_0^2 \cos(2\kappa L) e^{-2j\beta L}}{1 - (r_0 \cos(\kappa L) e^{-j\beta L})^2}, \quad (11)$$

with r_0 as the reflection of the plasmon mode at the end of a graphene sheet (also in the cavity ribbon). The final system requires that the mode transmitted in port 2 is reflected, so with $s_{2+} = r_0 s_{2-}$ in Eq. (9) one finds for the total reflection

$$R = \left| \frac{s_{1-}}{s_{1+}} \right|^2 = \left| S_1 + \frac{r_0 S_x^2}{1 - r_0 S_3} \right|^2. \quad (12)$$

The reflection is then determined by the parameters L and x_2 that we discuss in the next section and also by β , κ , and r_0 . The latter one was mentioned in the previous section and was relatively constant with the frequency and the doping. The coupling constant κ is fitted from simulations of a directional coupler composed of two sheets of graphene separated a distance d using Eqs. (7) and (8). Finally, the plasmon dispersion is known from simulations. We already discussed the real part of the propagation constant $\Re(\beta)$ in Fig. 4.

B. Results and Discussion

First we examine the effect of x_2 , the distance between the side ribbon and the end of the semi-infinite sheet. The total size of the system $x_1 + L + x_2 = 200$ nm is kept constant. By fitting simulations we obtain $\kappa \approx 9$ rad/m when $d = 30$ nm and the graphene is 1 eV doped. Note that varying the distance d changes κ (for example $\kappa \approx 15$ rad/m for $d = 20$ nm) and one can tune resonance frequencies with this parameter (not shown here). Note also that we chose to work with high doping ($E_F = 1$ eV) to reduce the size of the structure and the computational time, but the same effect is observed for smaller doping levels at higher wavelengths.

Figures 6(a) and 6(b) show, respectively, the simulated and theoretical reflection as a function of wavelength λ and the position of the cavity x_2 for a cavity length $L = 30$ nm. First, one observes a good agreement of simulations with theory. Next, we observe a general augmentation of the reflection with increasing wavelength. Indeed, because of the interband transitions, losses are less important at larger wavelengths: the propagation length of the plasmon is greater and the reflection becomes larger.

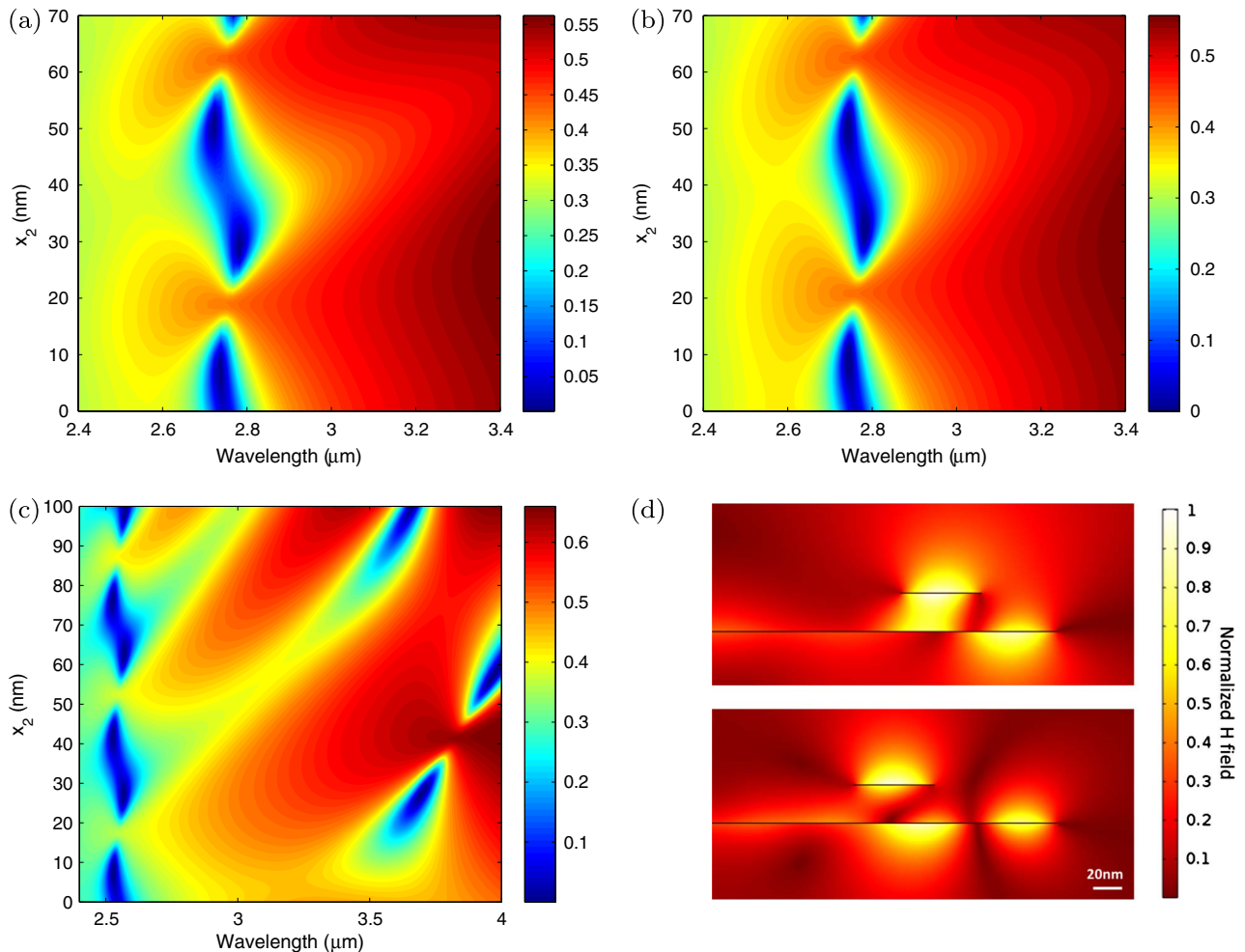


Fig. 6. Map of the (a) simulated and (b) theoretical reflection of the system with a $L = 30$ nm length cavity varying the wavelength and its position (x_2). The blue zones represent the reflection minima of the first-order cavity mode. (c) Theoretical map for a cavity length $L = 60$ nm. One observes the second-order minima for small wavelengths and the symmetric- and antisymmetric-type resonances for higher wavelengths. (d) Normalized $|H_z|$ field of the cavity $L = 60$ nm, for two different resonances: the symmetric (up, with $x_2 = 57$ nm and $\lambda = 4.05$ μm) and antisymmetric (down, with $x_2 = 92$ nm and $\lambda = 3.53$ μm) mode, respectively.

Let us focus on the minima of the map (blue zones). As a first approximation, one can predict the resonant wavelengths as explained for the isolated ribbon in the previous section via Eq. (6). In this way, the expected wavelength would be $\lambda = 2.8 \mu\text{m}$ which is close to what is observed. However, with the directional coupling and the semi-infinite sheet reflection, there is an interference via two other parameters: the coupling constant κ and x_2 .

First of all, for some values of x_2 (e.g., $x_2 = 20$ and 61 nm), there are no resonances. This stems from the half-plasmon wavelength $\lambda_p/2 = 41$ nm. Indeed, when there is no cavity, there is a stationary wave on the ribbon with incoming and reflected waves. Subsequently, if the cavity is centered on top of a node, the resultant field in the cavity will be very small: the forward incoming wave and the backward reflected wave create destructive interference in the cavity.

When the cavity is not centered on a node, different possible interferences appear depending on the cavity position and the coupling strength κ . An interpretation is provided by the supermodes of the directional coupler. Depending on the position of the cavity, one will excite the symmetric [large field between the graphene sections, Fig. 6(d) (up)] or anti-symmetric [node between the graphene sections, Fig. 6(d) (down)] supermode. The two supermodes have a different plasmon dispersion leading to two corresponding wavelengths. This is why we observe a slanted shape of the blue zone, with two reflection dips, e.g., at $\lambda = 2.75 \mu\text{m}$ ($x_2 = 10$ nm) and at $\lambda = 2.78 \mu\text{m}$ ($x_2 = 28$ nm).

As the supermodes differ more when κ is large, the wavelength gap between the reflection dips becomes larger, see Fig. 6(c), which shows the reflection in function of λ and x_2 for a larger cavity length $L = 60$ nm. Indeed, a larger cavity size implies a larger resonance wavelength ($\approx \lambda_p/2$) and so a larger coupling κ (the plasmon is less confined transversally and it interacts more with the other ribbon). In this case, one observes a larger wavelength gap between two minima ($\lambda = 3.7 \mu\text{m}$, $x_2 = 27$ nm, and $\lambda = 3.95 \mu\text{m}$, $x_2 = 53$ nm). The other blue zones observed around $\lambda = 2.5$ – $2.6 \mu\text{m}$ are second-order resonances.

Finally, we investigate the reflection tunability of such a structure. The reflection as a function of the wavelength is plotted for different doping levels of the cavity ribbon in Fig. 7.

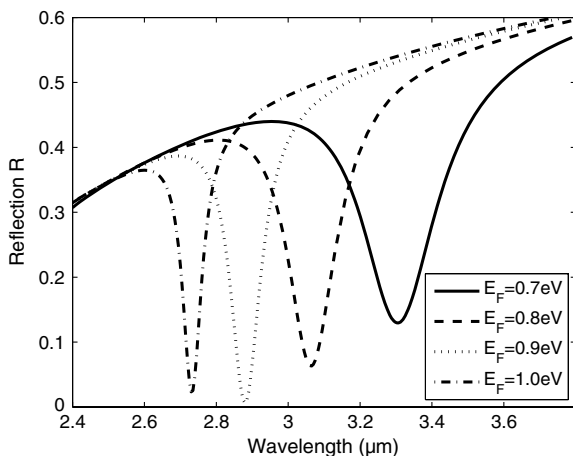


Fig. 7. Reflection as a function of the wavelength for different doping levels of the graphene ribbon cavity. One observes the tunability of the reflection dip with E_F .

The doping level of the access waveguide is fixed to 1 eV and the one of the cavity ribbon is modified from 0.7 to 1 eV. One clearly sees a shift in the reflection dip from $\lambda = 3.3$ to $2.75 \mu\text{m}$. Here, a minimum of reflection ($R = 2.5\%$) can be reached for $E_F = 0.93$ eV when $\lambda = 2.84 \mu\text{m}$.

The tuning behavior is explained in a first approximation by the phase resonance condition of Eq. (6) as previously discussed (Section 2.B). A more accurate model can be developed similar to Section 3.A for two dissimilar waveguides. The tunability of such a structure can be realized via electrostatic gating of the graphene nanoribbon.

4. CONCLUSION

In conclusion, we show tunable reflection minima using nanocavities constructed by graphene ribbons. When the cavity is aligned with the semi-infinite sheet, there is a coupling of the plasmon depending on the distance, the losses, and very interestingly, the graphene doping. This leads to tunable wavelength selectors easily performed by changing an applied gate voltage, which is useful for optoelectronic applications, even if the quality factor is of the order of more traditional plasmonic devices. The coupling is fully explained by coupled mode theory and the resonance condition is modeled via the graphene plasmon dispersion.

When the cavity is on top of a semi-infinite sheet of graphene, the reflection resonances depend on the vertical distance and the horizontal position of the cavity, the cavity size, and the graphene doping. The theory of directional couplers is in good agreement with the simulated results. We show that the horizontal position of the cavity plays an important role creating or annihilating the resonance. The coupling constant is also essential, giving two resonant wavelengths for two different positions because of the symmetric and antisymmetric supermodes. Finally, we illustrate the strong tunability of the reflection thanks to the doping level of graphene. This work aids in the design of ultracompact optoelectronic devices utilizing nanoscale graphene cavities.

ACKNOWLEDGMENTS

This work is supported by the Belgian Science Policy Office under the project “Photonic@be” (P7-35) and by the Fonds National de Recherche Scientifique (FNRS) in Belgium.

REFERENCES

1. J. Zhu, M. Chen, Q. He, L. Shao, S. Wei, and Z. Guo, “An overview of the engineered graphene nanostructures and nanocomposites,” *RSC Adv.* **3**, 22790–22824 (2013).
2. D. Hecht, L. Hu, and G. Irvin, “Emerging transparent electrodes based on thin films of carbon nanotubes, graphene, and metallic nanostructures,” *Adv. Mater.* **23**, 1482–1513 (2011).
3. Y. Yang, A. M. Asiri, Z. Tang, D. Du, and Y. Lin, “Graphene based materials for biomedical applications,” *Mater. Today* **16**(10), 365–373 (2013).
4. A. Vakil and N. Engheta, “Transformation optics using graphene,” *Science* **332**, 1291–1294 (2011).
5. F. Bonaccorso, Z. Sun, and A. Ferrari, “Graphene photonics and optoelectronics,” *Nature Photonics* **4**, 611–622 (2010).
6. G. Jo, M. Choe, S. Lee, W. Park, Y. Kahng, and T. Lee, “The application of graphene as electrodes in electrical and optical devices,” *Nanotechnology* **23**, 112001 (2012).
7. P.-Y. Chen, J. Soric, and A. Alù, “Invisibility and cloaking based on scattering cancellation,” *Adv. Opt. Mater.* **24**, OP281–OP304 (2012).

8. A. N. Grigorenko, M. Polini, and K. Novoselov, "Graphene plasmonics," *Nat. Photonics* **6**, 749–758 (2012).
9. P. Avouris and M. Freitag, "Graphene photonics, plasmonics, and optoelectronics," *IEEE J. Sel. Top. Quantum Electron.* **20**, 6000112 (2014).
10. Q. Bao and K. Loh, "Graphene photonics, plasmonics, and broadband optoelectronic devices," *ACS Nano* **6**, 3677–3694 (2012).
11. M. Jablan, H. Buljan, and M. Soljacic, "Plasmonics in graphene at infrared frequencies," *Phys. Rev. B* **80**, 245435 (2009).
12. Z. Q. Li, E. A. Henriksen, Z. Jiang, Z. Hao, M. C. Martin, P. Kim, H. Stormer, and D. N. Basov, "Dirac charge dynamics in graphene by infrared spectroscopy," *Nat. Phys.* **4**, 532–535 (2008).
13. J. Christensen, A. Manjavacas, S. Thongrattanasiri, F. H. L. Koppens, and F. J. G. de Abajo, "Graphene plasmon waveguiding and hybridization in individual and paired nanoribbons," *ACS Nano* **6**, 431–440 (2012).
14. X. Zhu, W. Yan, N. A. Mortensen, and S. Xiao, "Bends and splitters in graphene nanoribbon waveguides," *Opt. Express* **21**, 3486–3491 (2013).
15. B. Wang, X. Zhang, X. Yuan, and J. Teng, "Optical coupling of surface plasmons between graphene sheets," *Appl. Phys. Lett.* **100**, 131111 (2012).
16. H. Lizuka and S. Fan, "Deep subwavelength plasmonic waveguide switch in double graphene layer structure," *Appl. Phys. Lett.* **103**, 233107 (2013).
17. W. B. Lu, W. Zhu, H. J. Xu, Z. H. Ni, Z. G. Dong, and T. J. Cui, "Flexible transformation plasmonics using graphene," *Opt. Express* **21**, 10475–10482 (2013).
18. L. Falkovsky and A. Varlamov, "Space-time dispersion of graphene conductivity," *Eur. Phys. J. B* **56**, 281–284 (2007).
19. L. Falkovsky, "Optical properties of graphene," *J. Phys.* **129**, 012004 (2008).
20. D. Efetov and P. Kim, "Controlling electron-phonon interactions in graphene at ultrahigh carrier densities," *Phys. Rev. Lett.* **105**, 265805 (2010).
21. V. Kravets, A. N. Grigorenko, R. Nair, P. Blake, S. Anissimova, K. Novoselov, and A. Geim, "Spectroscopic ellipsometry of graphene and an excitation-shifted van Hove peak in absorption," *Phys. Rev. B* **81**, 155413 (2010).
22. G. Pirruccio, L. Moreno, G. Lozano, and J. Rivas, "Coherent and broadband enhanced optical absorption in graphene," *ACS Nano* **7**, 4810–4817 (2013).
23. S. Fan, W. Suh, and J. Joannopoulos, "Temporal coupled-mode theory for the Fano resonance in optical resonators," *J. Opt. Soc. Am. A* **20**, 569–572 (2003).
24. H. A. Haus, *Waves and Fields in Optoelectronics* (Prentice-Hall, Inc., 1984).
25. K. Novoselov, A. Geim, S. Morozov, D. Jiang, Y. Zhang, S. Dubonos, I. Grigorieva, and A. Firsov, "Electric field effect in atomically thin carbon films," *Science* **306**, 666–669 (2004).
26. P. West, S. Ishii, G. Naik, N. Emani, V. Shalaev, and A. Boltasseva, "Searching for better plasmonic materials," *Laser Photonics Rev.* **4**, 795–808 (2010).
27. B. E. A. Saleh and M. C. Teich, *Fundamentals of Photonics* (Wiley, 2007).